Bulk Band Gaps in Divalent Hexaborides

J. D. Denlinger
Advanced Light Source, Lawrence Berkeley National Laboratory, Berkeley, California 94720

J. A. Clack, J.W. Allen, and G.-H. Gweon
Randall Laboratory, University of Michigan, Ann Arbor, Michigan 48109-1120

D. M. Poirier* and C. G. Olson
Ames Laboratory, Iowa State University, Ames, Iowa 50011

J. L. Sarrao,† A. D. Bianchi,† and Z. Fisk
National High Magnetic Field Lab and Department of Physics, Florida State University, Tallahassee, Florida 32306
(Received 20 July 2001; published 20 September 2002)

Complementary angle-resolved photoemission and bulk-sensitive *k-resolved* resonant inelastic x-ray scattering of divalent hexaborides reveal a > 1 eV X-point gap between the valence and conduction bands, in contradiction to the band overlap assumed in several models of their novel ferromagnetism. This semiconducting gap implies that carriers detected in transport measurements arise from defects, and the measured location of the bulk Fermi level at the bottom of the conduction band implicates boron vacancies as the origin of the excess electrons. The measured band structure and X-point gap in CaB_6 additionally provide a stringent test case for many-body quasiparticle band calculations.

DOI: 10.1103/PhysRevLett.89.157601 PACS numbers: 79.60.–i, 71.18.+y, 71.20.–b

Great interest in the divalent hexaborides has been generated recently by the discovery of ferromagnetism in La-doped CaB_6 [1] and by exotic theoretical models to explain the unusual magnetism, e.g., that it represents the ground state of a dilute electron gas [2,3] or of a doped excitonic insulator [4–7]. Subsequent experiments have extended the observation of ferromagnetism also to the undoped systems of CaB_6, SrB_6, and La-doped BaB_6 [8–10] raising new questions about the origins of the unusual magnetism.

Central to the excitonic instability model, and indeed the starting point of most thinking about the divalent hexaborides, is the presumed existence of small band overlap between the top of the boron valence states and the bottom of the cation d-conduction band at the X point of the simple cubic Brillouin zone appropriate to these materials. Band overlap is predicted by local density approximation (LDA) band structure calculations [11–13], and de Haas–van Alphen (dHvA) and Shubnikov–de Haas (SdH) experiments [14–16] have been interpreted in this semimetal framework.

The well-known need for many-body corrections to the LDA in calculating semiconductor band gaps [17] calls into question the LDA band-overlap result. Indeed, a recent pseudopotential GW quasiparticle band calculation for CaB_6 has predicted a large 0.8 eV X-point band gap [18]. In contrast, two new all-electron GW calculations have instead predicted an intermediate 0.3 eV bandgap [19] and an unusual increased band overlap relative to LDA [20], the latter thought to be due to the special character of the X-point states. The wide disparity in results for three different implementations of the GW quasiparticle band calculation scheme, which has been very successful for calculating band gaps in many common semiconductors [17], shows clearly that existing methodologies are inconsistent [21,22], applied in this case to a system with which there is no prior experience or firm experimental knowledge. Thus the question of band overlap versus a band gap (and its magnitude) is not only crucial for the novel physics of these materials but also serves as a particularly pointed test case for many-body quasiparticle band calculations.

In this paper we present data on divalent hexaborides from angle-resolved photoemission (ARPES) and resonant inelastic x-ray scattering (RIXS) showing a global *bulk* electronic structure consistent with the calculated bulk boron-block band structure, including the existence of a > 1 eV X-point band gap that is significantly larger than any of the three GW band calculations. For stoichiometric material there are just enough electrons to fill the boron-block bands so an X-point gap makes the material an insulator, whereas band overlap makes it a semimetal with hole and electron Fermi surfaces that enclose equal volumes. Thus the new band gap model, first suggested to the community by Ref. [16] and experimentally confirmed here, requires the reinterpretation of previous bulk-sensitive experiments [14–16,23–25] and also the recognition that the presence of measured metallic carrier densities of $\approx 10^{19}$–10^{20} cm^{-3} can be explained only by off-stoichiometry. Furthermore, Fermi surfaces measured by ARPES for SrB_6 and EuB_6 locate the chemical potential in the bottom of the conduction band and identify the carriers as n type, consistent with the sign of the Hall coefficient [24]. Additionally, it is found that the

chemical potential is variable from sample to sample and is also surface dependent, not surprising for a defect dominated semiconductor. The observed excess electrons imply either excess cations or boron vacancies, almost certainly the latter since it is not likely that excess metal ions can be packed into the rigid B_6 sublattice. While such boron vacancies may also produce the magnetic moments [26], recent detection of Fe impurities correlated to magnetism suggest an alternate origin [27], and both possibilities suggest some similarities to dilute magnetic semiconductors [28].

Single crystal samples of CaB_6, SrB_6, and EuB_6 were grown from an aluminum flux using powders prepared by boro-thermally reducing cation oxides [23]. ARPES experiments were performed both at the undulator beam line 10.0 of the Advanced Light Source (ALS) synchrotron and at the Ames/Montana beam line of the Synchrotron Radiation Center (SRC) at the University of Wisconsin. Samples oriented by Laue diffraction were cleaved *in situ* to reveal a [100] surface just before the measurement, which was done at a sample temperature of 20–30 K and in a vacuum of $\approx 4 \times 10^{-11}$ Torr. A photon energy of 30 eV was used to probe the Γ-X band structure, a value internally consistent with an "inner potential step" of 11.2 eV experimentally determined for EuB_6 from photon energy dependent measurements. The Fermi energy (E_F) and instrumental resolution were calibrated with a reference spectrum taken on scraped Au or sputtered Pt foils. The ALS instrumental resolution was 22 meV with total angular resolution of 0.3°. The SRC instrumental resolution was 130 meV with an angular resolution of ±1°. Fermi-energy intensity maps [or "Fermi surface" (FS) maps] were acquired by detection of electron emission along two orthogonal detection angles relative to the fixed sample position. The energy window for the SRC FS maps was 170 meV.

Bulk-sensitive soft x-ray emission (SXE) and absorption (XAS) spectroscopies were performed at the ALS Beamline 8.0 with experimental emission and absorption spectral resolutions of ≈ 0.3 eV and ≈ 0.1 eV, respectively. SXE, measured with a 1500 lines/mm grating spectrometer for fixed photon energy excitation at and above the B 1*s* core threshold, is used as a probe of the dipole-selective occupied valence band (VB) partial density of states (DOS), i.e., boron *p* states. In the RIXS regime near threshold, momentum conservation between valence and conduction electrons in the final state provides *k-resolved* features in the valence SXE [29]. XAS, a probe of unoccupied conduction band (CB) states, was measured both by total electron yield (TEY) as a function of photon energy and by partial fluorescence yield (PFY), detecting the entire VB emission.

Figure 1 shows the band structure measured at the ALS for CaB_6 along Γ-X compared to the pseudopotential *GW* band calculation [18]. The ARPES data, shown with reverse gray-scale intensities, is the sum of two data sets with *s*- and *p*-polarization geometries that individually exhibit strong symmetry selection rule effects that we will present and analyze elsewhere. All boron-derived theory bands (1–6) are easily identified as labeled in Fig. 1 [30]. The valence band labeled "1" is observed to lie 1.15 eV below E_F, while the theory conduction band 0 is not observed. This indicates that, indeed, it is separated by a gap from valence band 1, and that the theory underestimates the band gap by at least 0.35 eV.

ARPES data always show the valence band structure of Fig. 1, including the *X*-point gap, but often the chemical potential is located in conduction band 0 above the gap to create a small *X*-point electron pocket. Figures 2(a) and 2(b) presents SRC data showing only the near E_F behavior for SrB_6 and EuB_6 with band labeling as in Fig. 1. Shown in Figs. 2(c) and 2(d) are k_x/k_y FS maps of the *X*-point electron pockets for the same surfaces as for the data of Figs. 2(a) and 2(b). The maps reveal an elliptical FS contour for EuB_6 and a smaller, not fully resolved, FS for SrB_6. As defined from peak positions marked in Fig. 2(a), the observation of the bottom of the conduction band allows a quantitative measure (1.15 ± 0.1 eV) of the *X*-point gap for SrB_6, approximately 40% larger than the maximum gap found in the CaB_6 *GW* band calculations. A similar gap value is inferred for EuB_6 in Fig. 2(b), but with larger uncertainty due to the visible smearing of spectral weight at the top of band 1. We ascribe this

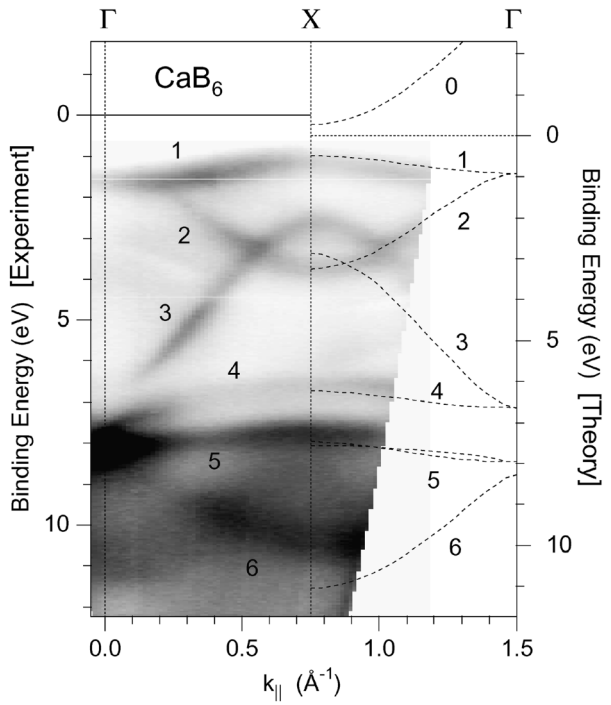

FIG. 1. Comparison of the experimental and theoretical band structures of CaB_6 along Γ-X. The reverse gray scale image of ARPES intensities is the sum of two data sets with 30 eV *s*- and *p*-polarized excitation. Dashed lines are from the quasiparticle *GW* calculation [18] giving *X*-point gap between bands 0 and 1.

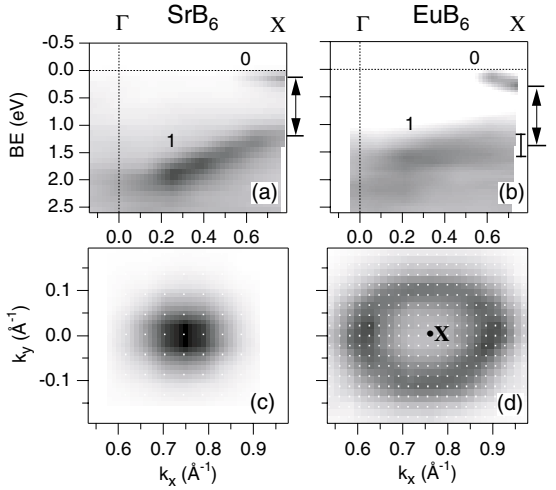

FIG. 2. Near-E_F valence band structure for (a) SrB_6 and (b) EuB_6 along Γ-X showing small band 0 electron pockets above the X-point gap to band 1. E_F intensity maps of the X-point at $h\nu = 30$ eV for (c) SrB_6 and (d) EuB_6 showing differing electron pocket sizes.

smearing, which occurs also for the other EuB_6 boron bands (not shown), but does not occur in CaB_6 and SrB_6 to the larger number of B vacancies in EuB_6 implied by the larger occupation of its X-point conduction band.

SdH and dHvA experiments on EuB_6 [14,15] also find ellipsoidal Fermi surfaces, i.e., two frequencies with the angle dependences [15] for the two extremal orbits, but with four frequencies total indicating two ellipsoids having slightly differing sizes. The semimetallic band-overlap model identifies these two FS sheets as the electron and hole pockets, while an alternate interpretation, consistent with our ARPES data, is that a single electron pocket is slightly spin split by the large internal field of the ferromagnetically ordered Eu $4f$ moments, aided by the very high magnetic field employed in the measurements [31]. Consistent with this interpretation, dHvA studies of CaB_6 and SrB_6 reveal only two frequencies [16] as expected for a single elliptical conduction band pocket. Of the more complex "lens" and "napkin ring" FS topologies resulting from band-overlap electron-hole mixing [11,13], only the lens FS has a possible dHvA correspondence [16] for CaB_6 and SrB_6, and both are precluded for EuB_6 by the observed SdH angular dependences.

Given the logical necessity for boron vacancies, it is then not surprising that considerable variation of the chemical potential position from sample to sample and from bulk to surface is a basic aspect of divalent hexaborides. For example, the FS dimensions found for EuB_6 by SdH and dHvA [14,15] are different both from one another and also from those implied by the ARPES of Fig. 2. In one ARPES experiment on EuB_6 an X-point electron pocket was initially not present and then appeared somewhat abruptly about 4 h after cleavage, but with a size smaller than that of Figs. 2(a) and 2(c). As expected if boron vacancies are involved, this time dependent shift of the surface chemical potential was accompanied by some redistribution and shift of the boron-block bands, but always with the *same* band gap value observed previously. Thus, as occurs for other semiconductors, surface defects and band bending control the surface chemical potential position. Elucidating and controlling the details of the defect states for both the bulk and the surface is an essential goal for future research.

Bulk-sensitive SXE and XAS *quantitatively* confirm the X-point band structure of CaB_6 presented in Fig. 1. Figure 3(a) compares valence emission spectra for CaB_6 with at-threshold (187.85 eV) and above-threshold (212 eV) excitation as indicated by arrows in the TEY absorption spectrum (Fig. 3, inset). The above-threshold SXE shows a line shape in very good agreement with a calculated boron p-DOS for SrB_6 [12]. The threshold-excited RIXS spectrum, on the other hand, has a different overall profile and multiple distinct peaks including a sharp elastic emission peak (labeled "e" in Fig. 3) at the threshold onset energy (187.85 eV) as the result of direct radiative decay from the CB minimum. This elastic peak provides a convenient marker for relative calibration of the emission and absorption energy scales [32]. The separation of the top of the VB emission from this absorption-threshold elastic peak is a graphic signature of the existence of a bulk band gap.

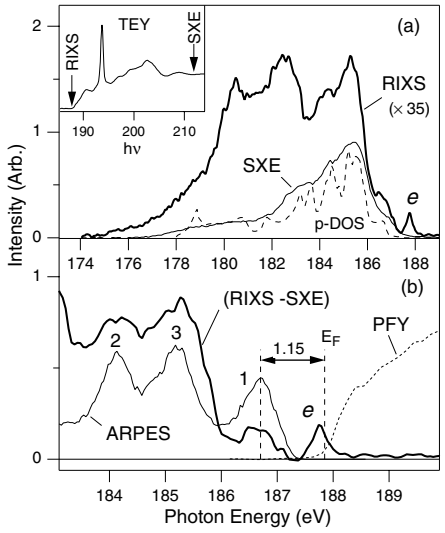

FIG. 3. (a) CaB_6 valence x-ray emission excited at-threshold (RIXS) and above-threshold (SXE) with comparison to calculated [12] boron p-DOS (dashed). (Inset) TEY absorption spectrum indicating excitation energies. (b) k-resolved RIXS difference spectrum (RIXS-SXE) with comparison to ARPES X-point spectrum showing alignment of valence band peaks and alignment of the ARPES Fermi level to the PFY absorption threshold.

Interpreted in the framework of RIXS, the threshold excitation into the *X*-point CB minimum results in a superposition of *coherent* momentum-conserving emission and *incoherent* emission of various origins [29]. As done in previous RIXS studies of semiconductors [33], we can refine the RIXS analysis to highlight the *k*-selective features if we approximate the incoherent emission profile by the above-threshold SXE spectrum and subtract it from the RIXS spectrum with the scaling shown in Fig. 3(a). The resulting RIXS difference spectrum is shown in Fig. 3(b) with comparison to the sharpest low binding energy peaks of the *X*-point CaB_6 ARPES spectrum plotted to align peaks 2 and 3. This alignment produces excellent agreement between ARPES and RIXS for peak 1, i.e., the VB maximum. Furthermore, the PFY absorption edge is also plotted in Fig. 3(b), and it is observed that the ARPES Fermi level occurs at the onset of the PFY threshold intensity rise. Thus for CaB_6, we have provided a bulk confirmation of all the features of the surface-sensitive ARPES measurements, in particular, the value of the *X*-point band gap (1.15 eV) and the location of the chemical potential just at the bottom of the conduction band. Soft x-ray measurements of other divalent hexaborides give similar results [34,35], and SXE and ARPES of La-doped CaB_6 and trivalent LaB_6 reveal that the gap magnitude is very sensitive to the conduction band occupation [35,36].

In summary, complementary ARPES and SXE/XAS experiments on divalent CaB_6 quantitatively agree to provide a clear case for the existence of a large energy scale bulk band gap. Small energy scale excitonic-insulator or hybridization gap models based on *X*-point band overlap are thus precluded. Widely differing band gap values from pseudopotential and all-electron *GW* calculations illustrate the insufficiency of current theory, and our high-quality ARPES bulk band structure of CaB_6 sets a clear benchmark for future work. The positioning of the bulk chemical potential in the conduction band and the resulting *n*-type carriers observed in nominally stoichiometric samples implicate boron vacancies. The physics of the divalent hexaborides is not that of an intrinsic semimetal, but that of a defect semiconductor.

J. W. A. thanks M. C. Aronson for stimulating his interest in these materials. We are grateful for very enlightening discussions with C. Kurdak, O. Gunnarsson, and E. Shirley. This work was supported at the University of Michigan by the U.S. DOE under Contract No. DE-FG02-90ER45416 and by the U.S. NSF Grant No. DMR-99-71611. The NHMFL is supported by the U.S. NSF Grant No. DMR-99-71348. The Ames Lab is supported by the U.S. DOE under Contract No. W-7405-ENG-82, and the SRC is supported by the U.S. NSF Grant No. DMR-00-84402. The ALS is supported by the U.S. DOE under Contract No. DE-AC03-76SF00098.

*Present address: Physical Electronics, Inc., 6509 Flying Cloud Drive, Eden Prairie, MN 55344.
†Present address: Los Alamos National Laboratory, Los Alamos, NM 87545.

[1] D. P. Young *et al.*, Nature (London) **397**, 412 (1999).
[2] D. Ceperley, Nature (London) **397**, 386 (1999).
[3] G. Ortiz, M. Harris, and P. Ballone, Phys. Rev. Lett. **82**, 5317 (1999).
[4] M. E. Zhitomirsky, T. M. Rice, and V. I. Anisimov, Nature (London) **402**, 251 (1999).
[5] L. Balents and C. M. Varma, Phys. Rev. Lett. **84**, 1264 (2000).
[6] V. Barzykin and L. P. Gor'kov, Phys. Rev. Lett. **84**, 2207 (2000).
[7] S. Murakami, R. Shindou, N. Nagaosa, and A. S. Mishchenko, cond-mat/0204640.
[8] P. Vonlanthen *et al.*, Phys. Rev. B **62**, 10 076 (2000).
[9] H. R. Ott *et al.*, Physica (Amsterdam) **281-282B**, 423 (2000).
[10] T. Terashima *et al.*, J. Phys. Soc. Jpn. **69**, 2423 (2000).
[11] A. Hasegawa and A. Yanase, J. Phys. C **12**, 5431 (1979).
[12] S. Massidda, A. Continenza, T. M. D. Pascale, and R. Monnier, Z. Phys. B **102**, 83 (1997).
[13] C. O. Rodriguez, R. Weht, and W. E. Pickett, Phys. Rev. Lett. **84**, 3903 (2000).
[14] R. G. Goodrich *et al.*, Phys. Rev. B **58**, 14 896 (1998).
[15] M. C. Aronson *et al.*, Phys. Rev. B **59**, 4720 (1999).
[16] D. Hall *et al.*, Phys. Rev. B **64**, 233105 (2001).
[17] M. S. Hybertson and S. G. Louie, Phys. Rev. Lett. **55**, 1418 (1985).
[18] H. J. Tromp *et al.*, Phys. Rev. Lett. **87**, 016401 (2001).
[19] M. van Schilfgaarde and T. Kotani (private communication).
[20] H. Kino *et al.*, Phys. Rev. B (to be published).
[21] T. Kotani and M. van Schilfgaarde, cond-mat/0111019.
[22] W. Ku and A. G. Eguiluz, Phys. Rev. Lett. **89**, 126401 (2002).
[23] H. R. Ott *et al.*, Z. Phys. B **102**, 337 (1997).
[24] Z. Fisk *et al.*, J. Appl. Phys. **50**, 1911 (1979).
[25] L. Degiorgi *et al.*, Phys. Rev. Lett. **79**, 5134 (1997).
[26] R. Monnier and B. Delley, Phys. Rev. Lett. **87**, 157204 (2001).
[27] K. Taniguchi *et al.*, cond-mat/0206101.
[28] Z. Fisk, H. R. Ott, V. Barzykin, and L. P. Gor'kov, Physica (Amsterdam) **312-313B**, 808 (2002).
[29] Y. Ma *et al.*, Phys. Rev. Lett. **69**, 2598 (1992).
[30] The weak broad dispersion at the bottom of the valence band, 11 eV at Γ, is suggestive of backfolding, perhaps consistent with 2×1 surface order seen in low energy electron diffraction of freshly cleaved surfaces.
[31] Our ARPES data are taken in zero field above $T_{\text{Curie}} \approx$ 15 K and so could not display the splitting.
[32] Absolute photon energies were calibrated to a 194.0 eV TEY peak due to surface boron oxide.
[33] J. Lüning *et al.*, Phys. Rev. B **56**, 13 147 (1997).
[34] J. D. Denlinger *et al.*, cond-mat/0107426.
[35] J. D. Denlinger (unpublished).
[36] S.-K. Mo *et al.*, Physica (Amsterdam) **312-313B**, 668 (2002).